Directed Graph Transformers

Anonymous authors
Paper under double-blind review

Abstract

In this paper, we address the problem of capturing graph directionality using transformers. Most existing graph transformers typically capture distances between graph nodes and do not take edge direction into account. This is a limiting assumption since many graph applications need to exploit sophisticated relationships in graph data, such as time, causality, or generic dependency constraints. We introduce a novel graph transformer architecture that explicitly takes into account the directionality between connected graph nodes. To achieve this, we make use of dual encodings to represent both potential roles, i.e., source or target, of each pair of vertices linked by a directed edge. These encodings are learned by leveraging the latent adjacency information extracted from a directional attention module, localized with k-hop neighborhood information. Extensive experiments on synthetic and real graph datasets show that our approach can have significant accuracy gains over previous graph transformer (GT) and graph neural network (GNN) approaches, providing state-of-the-art (SOTA) results on inherently directed graphs.

1 Introduction

Graphs are one of the most general and versatile data structures that are encountered in diverse application domains, ranging from biology and social networks to transportation and finance. Analyzing the graphs that arise from such applications and discovering patterns in them is of paramount importance in the associated domains. An important property of a graph is whether its edges are directed or not. Directed graphs are natural representations of relations including social connections, human communications, paper citations, financial transactions, Web links, and causes and effects. The state-of-the-art methods for analyzing directed graphs use Graph Neural Networks (GNNs) to learn node and directed edge encodings for tasks like link prediction (Kollias et al., 2022; Salha et al., 2019), node classification (Zhang et al., 2021) and graph-level tasks (Beaini et al., 2021).

In this paper, we address the relatively unexplored problem of analyzing *directed* graphs using graph transformers (GTs). Transformers hold the promise of enhanced performance over GNNs due to their ability to represent entities without enforcing the inductive adjacency bias (Vaswani et al., 2017), and due to their *dynamic* multi-head attention mechanism, in contrast to GNNs where the attention is hardwired in *static* edge weights. This flexibility of GTs comes, however, with the challenge of modeling directed graph structures. Most existing GTs focus on integrating only the graph connectivity structure into the Transformer. They do not prioritize how to reflect the directionality of graph edges in their proposed architecture. This is either due to the fact that some key techniques are not applicable to directed graphs (e.g., Laplacian eigenvectors (Dwivedi & Bresson, 2021)) or the edge-direction information is encoded as static, fixed scalars (either local in/out degrees in (Ying et al., 2021) or pairwise shortest path distances in (Hussain et al., 2022; Ying et al., 2021)).

We introduce *Directed Graph Transformer* (DiGT), a novel GT architecture that explicitly takes into account graph directionality. The crux of this architecture is that it incorporates both edge direction and graph connectivity structure into the standard Transformer architecture (Vaswani et al., 2017) as first-class citizens. Edge direction is represented by dual encodings for each graph node capturing its potential role as either a source or target of a directed edge. Source and target encodings are learned using a multi-head *directional attention* module that incorporates edge channels as bias. By interpreting attention matrices as latent

adjacency matrices, our technique updates a node's source vector by aggregating the target vectors of the neighbors it points to, after incorporating suitable learnable parameters; similarly, a node's target vector update is the aggregation of the source vectors of those neighbors pointing to it.

Although the general idea of using dual encodings at each graph node has been explored in various non-GT methods for directed graph learning, its application to the domain of GTs is novel and comes with its challenges. The main difference is that existing methods leverage and rely on the existing directed graph structure: the dual encodings are statically computed based on graph properties or message passing occurs using the directed graph connectivity structure. This introduces a convolutional inductive bias: the neighborhood of a node only consists of the edges of the directed graph and cannot include latent edges which could be learned and produce more discriminative node encodings for directed graphs. In contrast, in DiGT dual node encodings are *dynamically* learned without using the explicit directed graph structure.

We evaluate our DiGT model architecture for directed graph classification tasks. A challenge is that publicly available directed graph benchmark datasets for this task are scarce and only capture directionality indirectly. For example, the directed graph dataset in (Hussain et al., 2022) is derived from `MNIST/CIFAR10` images which are inherently undirected. To this end, we introduce the `FlowGraph` family of directed graph datasets that explicitly relate the edge direction pattern in graphs to their classification labels. Using these new datasets, as well as existing `MNIST/CIFAR10` (Hussain et al., 2022), `Twitter` (Leskovec & Mcauley, 2012), and `Malnet-tiny` (Freitas et al., 2020) datasets, we empirically demonstrate that DiGT gives significant accuracy gains for the tasks on both synthetic and real graph datasets. Our extensive experiments reveal that when edge directionality is an inherent, rather than derivative, characteristic of the instances to be classified, DiGT provides state-of-the-art (SOTA) results, outperforming graph transformer based and GNN alternatives by a large margin.

2 Related work

Methods for Directed Graph Learning. Earlier works on analyzing directed graphs are based on matrix factorization techniques to learn node encodings, such as Singular Value Decomposition (SVD) of higher-order adjacency matrices exploring the directed k-hop neighborhood of a node (Ou et al., 2016), or Non-negative Matrix Factorization (NMF) (Sun et al., 2019). Another line of work focuses on analyzing special matrix forms of adjacency information such as the Hermitian adjacency matrix of the directed graph (Cucuringu et al., 2020) or learning linear combinations of powers of the directed graph adjacency matrix and its transpose (He et al., 2021). APP (Zhou et al., 2017) uses random walks with restart as a tool to scale to large graphs and harvests asymmetric and high-order similarities between node pairs. More recently, GNNs have been used (Kollias et al., 2022; Tong et al., 2020a;b; Zhang et al., 2021) that operate based on a message-passing architecture and provide higher learning flexibility due to the usage of learnable weight matrices that multiply the node encodings. Graph Attention Network (GAT) (Veličković et al., 2017) is a GNN that incorporates local self-attention resembling a transformer.

A limitation of all the aforementioned approaches is that they critically rely on the explicit directed graph structure (adjacency matrix): (a) The k-hop neighborhood learning techniques (He et al., 2021; Ou et al., 2016; Sun et al., 2019; Zhou et al., 2017) involve matrix factorization or composition of powers of known adjacency matrices, or random walks over the graph structure. (b) Special matrix forms of adjacency information used in (Cucuringu et al., 2020; Tong et al., 2020a) require the directed graph as input. (c) GNNs in (Kollias et al., 2022; Salha et al., 2019; Tong et al., 2020b; Veličković et al., 2017; Zhang et al., 2021) are message-passing models, and single or dual-node encoding messages can flow only through existing edges. Reliance on the directed graph structure introduces inductive bias during learning: latent edges that could positively contribute to the learning problem at hand can be missed as a result. In contrast, DiGT does not rely on the directed graph structure (in effect it assumes full graph connectivity) and learns the edge weights by exchanging the dual node encodings between the nodes.

We note here that the general idea of dual node encodings has also been used in several of the above works. However, such encodings are typically computed by exploiting the directed graph structure. Applying this idea in GTs is challenging because there are no assumptions on graph structure (i.e., assuming full connectivity) and they need to be learned in a dynamic manner.

Graph Transformers GTs were introduced in (Dwivedi & Bresson, 2021), which proposed two inspiring GT architecture variants. The first variant produces only node encodings, while the second variant is augmented to also produce edge encodings. Node encodings follow the standard Transformer architecture (Vaswani et al., 2017), while edge encodings are updated by scaling the attention matrix. They attend only to existing neighbors (local self-attention), so a strong inductive bias is enforced. SAN (Kreuzer et al., 2021) uses learned positional encodings (LPE) to enhance the learning of graph structure. SAT (Chen et al., 2022) enhances the learning by extracting k-hop subgraphs. In Graphormer (Ying et al., 2021), the attention aperture critically expands to all nodes (global self-attention). They propose adding and learning node encodings that are functions of input and output degree centralities (centrality encoding), and arbitrary node pairs are represented by two bias terms to the attention matrix (spatial and edge encodings). In Edge-Augmented Transformer (EGT) (Hussain et al., 2022), they combine ideas from (Dwivedi & Bresson, 2021) (separate channels for nodes and edges, scaling and gating the attention matrix) and from (Ying et al., 2021) (global self-attention, bias terms from spatial encoding, however, learned from the edge channels) to yield an effective GT approach. Recently, hybrid models that combine graph neural networks with graph transformers have been proposed, such as GraphGPS (Rampášek et al., 2022) and Exphormer (Shirzad et al., 2023), that attain competitive performance results, while aiming at scalability. GraphGPS is a framework for combining pluggable encodings, local message passing, and global attention modules; Exphormer introduces a sparse attention mechanism based on global virtual nodes and expander graphs. In (Geisler et al., 2023), they learn directed graphs using Transformers, which leverage special positional encodings based on Magnetic Laplacian eigenvectors (Furutani et al., 2020) and random walks.

Our DiGT approach is a global self-attention transformer, learning both dual node encodings and edge encodings (dual-channel architecture). A node encoding in DiGT consists of a pair of source and target vectors that capture the edge direction semantics. Therefore, in downstream tasks that require directionality and take node encodings as input, DiGT provides embeddings of high discriminative power. In comparison, Graphormer (Ying et al., 2021), EGT (Hussain et al., 2022), and the other graph transformers (Dwivedi & Bresson, 2021; Zhang et al., 2020) produce only single-vector node embeddings that cannot differentiate the direction of an edge; and, as already mentioned, directed GNNs (Kollias et al., 2022; Salha et al., 2019; Tong et al., 2020b; Veličković et al., 2017; Zhang et al., 2021) produce dual node embeddings that suffer from convolutional inductive bias, that is restricted to only the given neighborhood structure.

3 Directed Graph Transformer Architecture

We now describe our directed graph transformer DiGT, whose main components are shown in Figure 1. DiGT uses three main ideas: dual node embeddings – for source and target representations, with a HITS-inspired (Kleinberg, 1999) aggregation combined with learnable implicit adjacency information via directed attention, as well as using k-hop neighborhood virtual edges. We will detail these ideas below. Our model contains multiple DiGT layers, as well as multiple heads for the attention. However, in the description below, we omit the layer and head notations for ease of presentation.

3.1 Input Layer

We represent a directed *graph* as $G(V, E)$; V is the set of $n = |V|$ graph nodes, $E = \{(i, j) \in V \times V : i \mapsto j\}$ is the set of its $m = |E|$ directed edges. Each node i is equipped with a pair of vectors in $\mathbb{R}^d$, $1 \leq i \leq n$: (i) vector $\mathbf{s}_i$ encodes i's role as a source, which is the same for any of the directed edges it participates in as a source, and (ii) vector $\mathbf{t}_i$ encodes i's role as a target.

Positional encodings play an important role in comprehending graph structures for GNNs. Traditional methods, such as the graph Laplacian, are limited to undirected graphs due to their requirements of a symmetric adjacency matrix. In our study, we select two techniques to overcome this limitation: Singular Value Decomposition (SVD), and the Magnetic Laplacian (Geisler et al., 2023). We detail these two positional encoding methods in the Appendix. For a given adjacency matrix $\mathbf{A}$, we denote by $\mathbf{S}_r$ and $\mathbf{T}_r$ the positional encodings for the source and target nodes, respectively. When input node features $\mathbf{X}_f$ are available (set

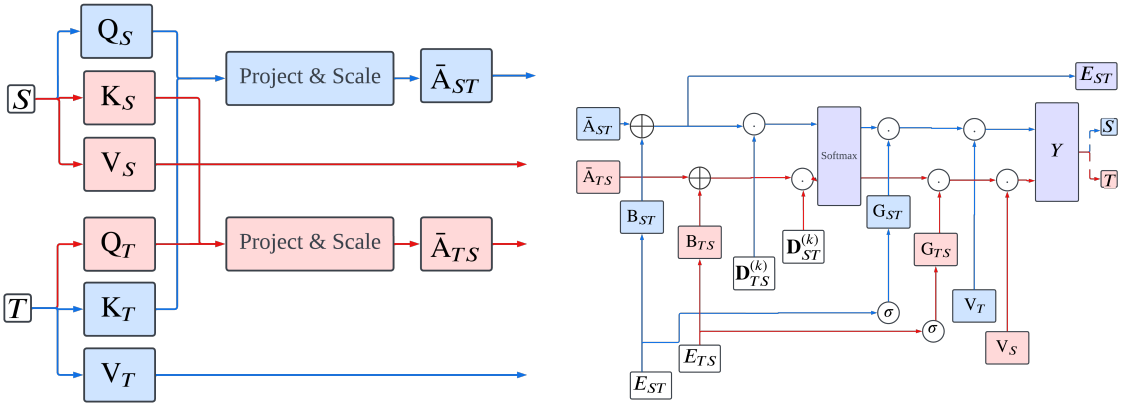

(a) DiGT source and target attention head

(b) DiGT layer structure

Figure 1: The two figures show the DiGT architecture. In (a), the attention is calculated in both directions for each node. Then, in (b), a softmax operation is applied on the stacking dimension to compute the importance of directionality (i.e., softmax is over the ST and TS axes). The white nodes represent input vectors, blue nodes and arrows represent the flow of source embeddings, red nodes and arrows represent the flow of target embeddings, and purple nodes represent the operations on both source and target embeddings.

$\mathbf{X}_f = 0$, otherwise), the input/initial *node* embeddings for the DiGT model are given as

$$\mathbf{S} = L_s(\mathbf{S}_r) + L_f(\mathbf{X}_f) \qquad \mathbf{T} = L_t(\mathbf{T}_r) + L_f(\mathbf{X}_f) \tag{1}$$

where L_s, L_t and L_f are learnable linear transformations (subscripted as s for the sources, t for targets, and f for input features), and $\mathbf{S}, \mathbf{T} \in \mathbb{R}^{n \times d}$. To encode the edges, considering input edge features $\mathbf{E}_f$ (set $\mathbf{E}_f = 0$ otherwise), the input/initial *edge* embeddings for the DiGT model are given as

$$\mathbf{E}_{ST} = L_e([\delta_{st}]_{s,t=1,\ldots,n}) + L_{ef}(\mathbf{E}_f) \tag{2}$$

where L_e is an embedding layer, L_{ef} is a learnable linear transformation, and δ_{st} is the shortest directed path distance from source s to target t, clipped at maximum k-hops (if t is not reachable from s, we set $\delta_{st} = k+1$). The result, $\mathbf{E}_{ST} \in \mathbb{R}^{n \times n \times d_e}$, is the matrix of d_e dimensional edge embeddings, and we set $\mathbf{E}_{TS}$ as the transpose of $\mathbf{E}_{ST}$ along the first two dimensions.

3.2 DiGT Attention Layer

Given the dual node encodings, we need to determine the relationship between the source and target encoding vectors of different nodes, which will be used for updates in our GT architecture. For this, we draw high-level inspiration from the HITS (Kleinberg, 1999) centrality algorithm that computes two scalar-valued *hub* and *authority* scores for each node in a directed graph – a source node with a high hub score refers to (or points to) target nodes that contribute relevant information (in our case, for learning), and thus gain elevated authority scores. Consider for the moment one-dimensional or scalar source and target node embeddings, s_i and t_i, which serve as the hub and authority score, respectively; we can express their relationship as $s_i = \sum_{i \mapsto j} t_j$ (i.e., good hubs point to good authorities) and $t_i = \sum_{j \mapsto i} s_j$ (i.e., good authorities are pointed to by good hubs).

Generalizing to our d-dimensional source and target encoding *vectors* $\mathbf{s}_i$ and $\mathbf{t}_i$, we could analogously write:

$$\mathbf{s}_i = \sum_j \mathbf{A}_{ij}\mathbf{t}_j \quad \text{and} \quad \mathbf{t}_i = \sum_j \mathbf{A}_{ji}\mathbf{s}_j.$$

We can write the above equations more compactly as $\mathbf{S} = \mathbf{A}\mathbf{T}$ and $\mathbf{T} = \mathbf{A}^\top\mathbf{S}$. Conceptually, $\mathbf{s}_i$ and $\mathbf{t}_i$ play the role of multi-dimensional hub and authority scores.

Implicit and Directed Adjacency via Attention: The key insight in DiGT is that we should not rely on the fixed adjacency matrix $\mathbf{A}$; rather, we should construct an *implicit* adjacency matrix, denoted $\bar{\mathbf{A}}$, by exploiting the attention mechanism. A straightforward approach to compute $\bar{\mathbf{A}}$ could be $\bar{\mathbf{A}} = \mathbf{S}\mathbf{T}^\top$. However, we need to make this learnable. To allow the flexibility of learning weight matrices for computing the implicit adjacency we use dual attention mechanisms. For the source nodes $\mathbf{S}$, let

$$\mathbf{Q}_S = \mathbf{S}\ \mathbf{W}_{QS} \qquad \mathbf{K}_S = \mathbf{S}\ \mathbf{W}_{KS} \qquad \mathbf{V}_S = \mathbf{S}\ \mathbf{W}_{VS} \tag{3}$$

and similarly for the target nodes $\mathbf{T}$, let

$$\mathbf{Q}_T = \mathbf{T}\ \mathbf{W}_{QT} \qquad \mathbf{K}_T = \mathbf{T}\ \mathbf{W}_{KT} \qquad \mathbf{V}_T = \mathbf{T}\ \mathbf{W}_{VT} \tag{4}$$

where all $\mathbf{W}$'s $\in \mathbb{R}^{d \times d_p}$ are learnable weight matrices, and d_p is the projection dimensionality (suitably scaled down, based on the number of heads). As shown in Figure 1a, we obtain a pair of attention matrices

$$\bar{\mathbf{A}}_{ST} = \left(\mathbf{Q}_S {\mathbf{K}_T}^\top\right) / \sqrt{d_p} \qquad \bar{\mathbf{A}}_{TS} = \left(\mathbf{Q}_T {\mathbf{K}_S}^\top\right) / \sqrt{d_p} \tag{5}$$

That is, the attention matrix $\bar{\mathbf{A}}_{ST}$ treats the source nodes as queries and the target as keys to compute their similarity, and vice-versa for $\bar{\mathbf{A}}_{TS}$ (see Figure 1a).

Edge Bias and Neighborhood Attention: We now allow for the edge channels to directly influence the attention by introducing a per head *bias* matrix, $\mathbf{B}_{ST} \in \mathbb{R}^{n \times n}$, and *gate* matrix, $\mathbf{G}_{ST} \in \mathbb{R}^{n \times n}$, both of which are linear transformations from the edge encodings $\mathbf{E}_{ST}$ (with added layer norms). Further, $\mathbf{B}_{TS}$ and $\mathbf{G}_{TS}$ are their transpose matrices, respectively.

Next, we *localize* the attention from node channels to the k-hop neighborhood around each node. This is implemented by masking the attention matrix along with the edge bias via an element-wise product with the binary *k-hop filter matrix*, defined as $\mathbf{D}^{(k)}_{i,j} = \{1 \textit{ iff } \delta_{ij} \leq k, 0 \textit{ iff } \delta_{ij} > k\}$, where δ_{ij} denotes the shortest path distance from node i to node j. Thus, the attention matrices, denoted $\tilde{\mathbf{A}}$, for this layer are given as:

$$\tilde{\mathbf{A}}_{ST} = \left(\bar{\mathbf{A}}_{ST} + \mathbf{B}_{ST}\right) \odot \mathbf{D}^{(k)}_{ST} \qquad \tilde{\mathbf{A}}_{TS} = \left(\bar{\mathbf{A}}_{TS} + \mathbf{B}_{TS}\right) \odot \mathbf{D}^{(k)}_{TS} \tag{6}$$

where $\mathbf{D}^{(k)}_{ST}$ and $\mathbf{D}^{(k)}_{TS}$ are the filter matrices in the two directions. This way we control the attention to be within the k-hop neighbors around each node.

Directional Attention: For any two nodes within a graph, our objective is to determine the direction of message passing between them. To achieve this, we compare the attention values in both directions. The larger of these values will indicate the predominant direction of message passing. Therefore, unlike traditional transformers that compute node importance via a softmax along each *row* of the attention matrix, we stack both $\tilde{\mathbf{A}}_{ST}$ and $\tilde{\mathbf{A}}_{TS}$ and compute the softmax along the stacking direction (Figure 1b visualizes this mechanism), given as

$$\tilde{\mathbf{A}}_{ST}, \tilde{\mathbf{A}}_{TS} = \texttt{softmax}(\tilde{\mathbf{A}}_{ST}, \tilde{\mathbf{A}}_{TS}). \tag{7}$$

Note that directional attention combined with the k-hop filter matrix $\mathbf{D}^{(k)}$ applies a *soft-thresholding* for unidirectional edges, as opposed to the hard-thresholding that is typically used when masking with $-\infty$. That is, if we were to set $\mathbf{D}^{(k)}_{i,j} = -\infty$ if $\delta_{ij} > k$, then information would flow only along the direction that exists, and it would ignore the opposite direction for unidirectional edges. We show conclusively in our ablation study in Section 4.3 that soft-thresholding yields better performance.

Finally, we enable the flow of information between nodes by gating their value representations prior to aggregation; this is realized as multiplication by the sigmoid function, $\sigma()$, of the entries in *gate* matrices, $\mathbf{G}_{ST}$ and $\mathbf{G}_{TS}$, resulting in

$$\mathbf{Y} = \left((\tilde{\mathbf{A}}_{ST} \odot \sigma(\mathbf{G}_{ST}))\ \mathbf{V}_T\right)\ +\ \left((\tilde{\mathbf{A}}_{TS} \odot \sigma(\mathbf{G}_{TS}))\ \mathbf{V}_S\right), \tag{8}$$

where $\mathbf{Y} \in \mathbb{R}^{n \times d_p}$ is the value representation for one head. So, when we have $h = d/d_p$ heads, we concatenate all of them (and add layer norm) to obtain the final value representation $\mathbf{Y} \in \mathbb{R}^{n \times d}$, for the next step. Also, the different DiGT layers do not share edge embeddings and this is also true for bias and gate matrices.

3.3 Output Layers and Prediction

One point to note is that, after each DiGT layer, we take the combined value encoding $\mathbf{Y}$, and we use layer normalization and feed-forward network modules with residual connections, to produce the node and edge encoding outputs for a DiGT layer. These outputs become inputs for the next layer. Thus, the updated dual encodings $\mathbf{S}$, $\mathbf{T}$ for the next layer are given as:

$$\mathbf{S} = f(L_{YS}(\mathbf{Y})) \qquad \mathbf{T} = f(L_{YT}(\mathbf{Y})), \tag{9}$$

where, L_{YS} and L_{YT} are two linear transformations followed by a non-linear activation f (with layer norms and residual connections). To obtain the updated edge embeddings $\mathbf{E}_{ST} \in \mathbb{R}^{n \times n \times d_e}$ for the next layer, we add together $\bar{\mathbf{A}}_{ST}$ and $\mathbf{B}_{ST}$ from all the h heads, and apply a learnable linear transformation and non-linearity, as follows:

$$\mathbf{E}_{ST} = f(L_E(\bar{\mathbf{A}}_{ST} + \mathbf{B}_{ST})) \tag{10}$$

Lastly, to obtain the final output node embeddings, we concatenate both the source and target embeddings, as follows: $\mathbf{X} = \texttt{concat}(\mathbf{S}, \mathbf{T})$. After the last DiGT layer is processed, the encodings $\mathbf{X}$ are driven through some final task-specific learning modules. These are typically multilayer perceptron layers (MLP) for tasks related to *node* and *edge* learning (node classification, link prediction), or pooling layers for *graph-level* learning (graph classification, graph regression). For the directed graph classification task, we use *global average pooling* as our main method for producing a representation/encoding of the whole graph; this is essentially the average of the final node encodings. We also experiment with the method of *virtual nodes* based pooling (Hussain et al., 2022): a clique of artificial nodes (virtual nodes) are added to each graph and connected to all its nodes (with the edge directed only from a graph node to the virtual nodes). After training, we average the concatenated source and target node embeddings of the virtual nodes and leverage the same final MLP layers for the downstream task. We examine the effects of these choices in the ablation studies.

4 Experiments

Our experiments were performed on NVIDIA V100 GPUs, with 32GB memory, using PyTorch. An anonymous link to our implementation is provided in the Appendix, which also contains additional experimental details.

4.1 Directed Graph Datasets

Table 1: Randomized directionality via edge flips: Model performance

Model	`MNIST`	`CIFAR10`	Model	`Ogbg-Code2`	Model	`Malnet-tiny`	`Malnet-sub`
EGT	98.17 +/- 0.09	68.70 +/- 0.41	DAG	20.2 +/- 0.2	Exphormer	94.02 +/- 0.21	79.71 +/- 0.37
EGT-Flip50	97.99 +/- 0.09	67.28 +/- 0.38	DAG-Flip50	19.0 +/- 0.1	Exphormer-Flip50	87.90 +/- 1.65	71.51 +/- 0.45

Model	`FlowGraph2`	`FlowGraph3`	`FlowGraph6`	`Twitter3`	`Twitter5`
DiGT	98.00 +/- 0.54	74.61 +/- 1.95	46.03 +/- 0.41	93.33 +/- 0.64	86.67 +/- 0.52
DiGT-Flip50	49.67 +/- 1.39	32.33 +/- 1.66	16.78 +/- 0.04	82.96 +/- 1.13	65.44 +/- 0.38

There are several directed datasets used in previous studies, such as `MNIST` (Achanta et al., 2012), `CIFAR10` (Krizhevsky et al., 2009), `Ogbg-Code2` (Hu et al., 2020), and `Malnet-tiny` (Freitas et al., 2020). See the Appendix for dataset statistics.

`MNIST` and `CIFAR10`: (Hussain et al., 2022) used `MNIST` and `CIFAR10` as collections of *directed* graph inputs for their *directed* graph classification task, following the introduction of these datasets in (Dwivedi et al., 2020). They are originally collections of images (respectively, of handwritten digits and objects) and not

graphs. In (Dwivedi et al., 2020), they convert an image to a directed graph by first segmenting the original image pixels into sets of (coarser-grained) SLIC superpixels (Achanta et al., 2012). Directionality in the edges then follows from the fact that if a superpixel i has *fewer* neighboring superpixels than one of its neighbors j, it will tend to connect to j rather than the other way around (i.e., $i \mapsto j$ will have more weight than $j \mapsto i$).

`Malnet-tiny` and `Malnet-sub`: Malnet-tiny (Freitas et al., 2020) provides a graph classification task for five different types of malicious software. It contains 5,000 graphs, and each graph contains less than 5,000 nodes. Its graph size is an obstacle for many graph transformers. We apply a filter to generate the Malnet-sub dataset: we choose the graphs with fewer than 500 nodes for training sets, and those with fewer than 2,000 nodes for both validation and test datasets. As a result, the Malnet-sub dataset contains 2,444 graphs. `Malnet-sub` dataset is more challenging than `Malnet-tiny` since it forces the models to effectively generalize from smaller graphs in the training data to larger, unseen graphs in the validation and testing phases[1].

`Ogbg-Code2`: The ogbg-code2 dataset is a collection of Abstract Syntax Trees (ASTs) from thousands of Python method definitions extracted from 13,587 different popular repositories on GitHub. Given the AST and node features, the goal is code summarization, i.e., to predict the sub-tokens forming the method name.

4.1.1 Importance of Direction: Random Flip Test

Even though the above datasets are purported to be directed, our analysis points out a severe limitation, namely, direction plays little to no role in these datasets, unfortunately.

To evaluate the role of directionality in these datasets, we designed a simple random flip test. In essence, for a given edge flip probability, say θ (e.g., $\theta \in \{0.25, 0.5\}$), we flip each edge (u, v) with probability θ during each of the training, validation and testing steps. If, even after randomizing the edge direction for θ fraction of the edges, a model consistently achieves accuracy comparable to that on the original dataset, this provides strong support that directionality is not a crucial factor for that dataset.

Table 1 shows the results with $\theta = 0.5$ (i.e., 50% of the edges are flipped). We use EGT (Hussain et al., 2022) on the `MNIST` and `CIFAR10` graphs, Exphormer (Shirzad et al., 2023), which is the SOTA on `Malnet-tiny`, and DAGformer (Luo, 2022), which is the top-performer on the `Ogbg-Code2` leaderboard (Hu et al., 2020). We observe that despite altering the direction of almost half of the edges on `MNIST`, `CIFAR10` and `Ogbg-Code2`, the results remain largely unaffected: predictive performance drops at most 0.42% for `MNIST`, 1.42% for `CIFAR10`, and 1.2% for `Ogbg-Code2` in absolute terms. These tiny differences indicate that directionality is not important for those datasets. On the other hand, there is a significant performance loss on `Malnet-tiny` and `Malnet-sub` indicating the importance of directionality for these. See the Appendix for results on different θ values and other models, too.

4.1.2 Inherently Directed Datasets

Having shown that existing datasets used to evaluate directed graph transformers violate their *raison d'être*, we propose two classes of inherently directed graphs (see Appendix for details of dataset generation).

`FlowGraph` datasets: We introduce a family of directed graph datasets that explicitly relate the edge direction pattern in graphs to their classification labels. In each graph, we create multiple clusters of nodes interconnected by random edges and arrange these clusters in a sequential order. For directed edges linking nodes in consecutive clusters, namely cluster l and cluster $l+1$, we define a directional flow: a set percentage $f\%$ of edges flow from cluster l to $l+1$, while the remaining $1-f\%$ edges flow in the reverse direction. These directional flow percentages vary across different classes. We generate three distinct graph datasets with $2, 3,$, and 6 classes. Detailed descriptions and methodologies of these datasets are provided in the Appendix. From Table 1, we can see the directionality is important in these datasets: `FlowGraph2` experiences a 48.33% drop in performance when 50% of the edges are reversed. Large drops are observed for the other FlowGraph datasets too.

[1]For example, the current state-of-the-art model, Exphormer (Shirzad et al., 2023), achieves a high accuracy of 93.38% on `Malnet-tiny`, while its performance drops to 79.71% accuracy on `Malnet-sub` when constrained to 100,000 parameters.

`Twitter` datasets: We use 973 directed ego-networks from Twitter[2], each corresponding to some user u (*ego*): the ego-network is between u's friends also referred to as *alters* (Leskovec & Mcauley, 2012). If nodes v_i, v_j are in u's ego-network then u follows them and if v_i follows v_j then there is a directed edge $v_i \mapsto v_j$ in the ego-network. We introduce perturbations to each of these real ego-networks where a perturbation can be either (i) *rewiring* of an existing edge, or (ii) *reversing* of the direction of an existing edge. Leveraging these perturbations, we create two distinct graph datasets: `Twitter3` with 3 classes and `Twitter5` with 5 classes. These classifications are based on varying percentages of perturbed edges. We can see that with 50% edge flipping ratio, we observe significant drops in performance: `Twitter3` shows an absolute drop of 9.37%, whereas `Twitter5` shows a drop of 21.23%, indicating that directionality plays an important role for these datasets.

4.1.3 Degree of Directionality

To further cement the role of directionality for a dataset, we propose another measure – the *degree of directionality*. Let SCC denote a strongly connected component in a directed graph (a maximal subset of mutually reachable nodes). Further, given the set of m SCCs of a directed graph, $\mathcal{S} = \{S_1, S_2, ..., S_m\}$, define the *SCC entropy* of the graph as follows: $E(\mathcal{S}) = -\sum_{i=1}^{m} p_i \log p_i$, where $p_i = |S_i|/n$, i.e., the distribution of SCC sizes. A low entropy means that most nodes are mutually reachable, and thus directionality is not expected to play a big role. On the other hand, larger SCC entropy values, with a maximum value of $\log n$, indicate smaller the reachable components, which means that directionality is clearly important.

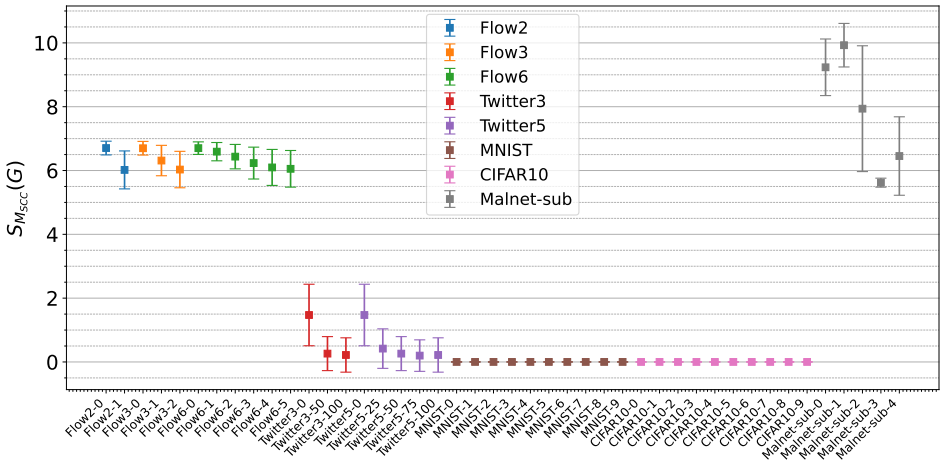

Figure 2: SCC Entropy Plot: The entropy for each class for each dataset is shown.

Figure 2 plots the SCC entropy for the different datasets; for each class, we plot the average and standard deviation[3]. We can see a very clear trend. `FlowGraph` classes are inherently directed, with larger entropies, and `Twitter` captures the inherent directionality of the "follow" relationship between entities, exhibiting lower entropy values. More importantly, the derived `MNIST` and `CIFAR10` have no inherent directedness, and their entropy values are extremely low. We will show that DiGT performs even better when direction matters, such as for `FlowGraph`, `Twitter`, and `Malnet-sub`.

4.2 Experimental Comparison

We compare DiGT with GCN (Kipf & Welling, 2016), GAT (Veličković et al., 2017), and PNA (Corso et al., 2020) as the representatives of GNNs, and with GT (Dwivedi & Bresson, 2021), SAN (Kreuzer et al., 2021), EGT (Hussain et al., 2022), and Exphormer (Shirzad et al., 2023) as the representatives of GTs. We train

[2] `https://snap.stanford.edu/data/ego-Twitter.html`

[3] We do not consider `ogb-code2` further, since directionality is not important for this dataset, and the task is code summarization instead of classification.

Table 2: *Classification accuracy of* DiGT *against various GNNs and GTs.*

Model	FlowGraph2	FlowGraph3	FlowGraph6	Twitter3	Twitter5	Malnet-sub	MNIST	CIFAR10
GCN (Kipf & Welling, 2016)	87.50 +/- 1.27	58.28 +/- 0.88	30.36 +/- 0.55	76.24 +/- 0.56	61.23 +/- 1.67	78.75 +/- 0.23	90.71 +/- 0.22	55.71 +/- 0.38
GAT (Veličković et al., 2017)	84.92 +/- 1.90	58.83 +/- 1.47	30.31 +/- 0.28	74.59 +/- 1.59	56.79 +/- 0.05	79.58 +/- 1.65	95.54 +/- 0.21	64.22 +/- 0.46
PNA (Corso et al., 2020)	96.17 +/- 0.31	72.94 +/- 0.64	41.42 +/- 1.32	88.26 +/- 1.16	70.94 +/- 2.01	78.85 +/- 1.01	97.41 +/- 0.16	70.21 +/- 0.15
GT (Dwivedi & Bresson, 2021)	93.17 +/- 0.82	66.17 +/- 0.60	36.20 +/- 1.12	90.66 +/- 0.35	79.55 +/- 0.68	75.04 +/- 0.61	97.75 +/- 0.12	68.02 +/- 0.16
SAN (Kreuzer et al., 2021)	91.73 +/- 1.84	63.87 +/- 0.66	34.57 +/- 0.45	85.33 +/- 0.78	63.13 +/- 1.65	79.27 +/- 0.23	96.82 +/- 0.13	66.96 +/- 0.39
EGT (Hussain et al., 2022)	95.00 +/- 1.67	72.06 +/- 1.16	42.97 +/- 0.62	86.49 +/- 0.73	73.94 +/- 1.47	72.35 +/- 1.38	98.17 +/- 0.09	68.70 +/- 0.41
Exphormer (Shirzad et al., 2023)	96.72 +/- 0.44	72.81 +/- 0.38	41.70 +/- 0.39	89.76 +/- 0.30	72.72 +/- 1.40	79.71 +/- 0.37	**98.55 +/- 0.04**	**74.69 +/- 0.13**
DiGT	**98.00 +/- 0.54**	**74.61 +/- 1.95**	**46.03 +/- 0.41**	**93.33 +/- 0.64**	**86.67 +/- 0.52**	**80.78 +/- 1.76**	98.02 +/- 0.10	67.05 +/- 0.20

them on `FlowGraph`, `Twitter`, `Malnet-sub`, and `MNIST/CIFAR10` respectively, restricted to 100K parameters. The accuracy results are listed in Table 2.

For `MNIST` and `CIFAR10`, which are not intrinsically directed by construction, DiGT maintains competitive performance over GT and EGT, experiencing only a minor decrease in accuracy. On the other hand, we observe that for all the datasets where direction is important, DiGT outperforms existing models providing SOTA results. For instance, on the `FlowGraph6` dataset, DiGT outperforms the next best model EGT by 3.06% in accuracy; the performance gains against GNN alternatives are even larger. Likewise, for the `Twitter5` dataset, DiGT outperforms the next best model, GT, by over 7.12% in accuracy. Among the GNNs, PNA is the best but lags behind DiGT by a huge margin. For `Malnet-sub`, models that are adept at capturing local information, such as GCN and Exphormer, show good performance. In contrast, traditional transformers that focus on the whole graph-level attention, like GT and EGT face more challenges for this task. However, DiGT surpasses the next best model, Exphormer, by 1.07% in accuracy. These results indicate that the dual attention mechanisms in DiGT can effectively learn both local and graph-level information.

4.3 Ablation Studies

We present ablation studies demonstrating the effectiveness of incorporating dual-vector attention matrices and k-hop virtual edge filters. Additionally, further ablation studies regarding other architectural components of our models, such as positional encodings and virtual nodes, are detailed in the Appendix.

4.3.1 Single-Vector Node Embeddings

To study the benefit of our dual node encodings, we constrain DiGT to leverage only one vector embedding per node, and refer to this version as DiGT-OneEmb. This kind of ablation makes DiGT similar to EGT, so the expectation is to get accuracy values closer to EGT. Results in Table 3 confirm this intuition. On average, the *ablated* DiGT model scores between the reported values for DiGT (higher) and EGT (lower) and much closer to those of EGT, especially in the case of `Twitter` datasets, e.g., 86.04 ± 0.45 versus 86.49 ± 0.73 in EGT for `Twitter3`.

Table 3: *Ablation: One Embedding.*

Model	FlowGraph2	FlowGraph3	FlowGraph6	Twitter3	Twitter5	Malnet-sub	MNIST	CIFAR10
DiGT	**98.00 +/- 0.54**	**74.61 +/- 1.95**	**46.03 +/- 0.41**	**93.33 +/- 0.64**	**86.67 +/- 0.52**	**80.78 +/- 1.76**	98.02 +/- 0.10	67.05 +/- 0.20
DiGT-OneEmb	96.75 +/- 0.41	73.67 +/- 0.85	43.81 +/- 0.42	87.52 +/- 0.50	73.09 +/- 0.59	70.07 +/- 1.30	97.49 +/- 0.72	66.78 +/- 0.90
EGT (Hussain et al., 2022)	95.00 +/- 1.67	72.06 +/- 1.16	42.97 +/- 0.62	86.49 +/- 0.73	73.94 +/- 1.47	72.35 +/- 1.38	**98.17 +/- 0.09**	**68.70 +/- 0.41**

Additionally, Figure 3 visually represents attention matrices for a sample graph within the `Malnet-sub` dataset. Figure 3(b) provides a pair of attention matrices in DiGT: the left figure shows the attention directed from the source to the target, namely $\tilde{\mathbf{A}}_{ST}$ in Equation 8, and the right one depicts the attention flow from the target to the source, namely $\tilde{\mathbf{A}}_{TS}$. Figure 3(c) shows the attention for the DiGT-OneEmb variant. For all the figures, we sum up the last layer of the attention matrices from all heads and normalize the values from 0 to 1. Brighter colors correspond to higher attention values, indicating greater importance of the information at that specific location. In summary, these figures visualize the status of the attention matrices, which are ready to be multiplied (after gating) by the values $\mathbf{V}_T, \mathbf{V}_S$.

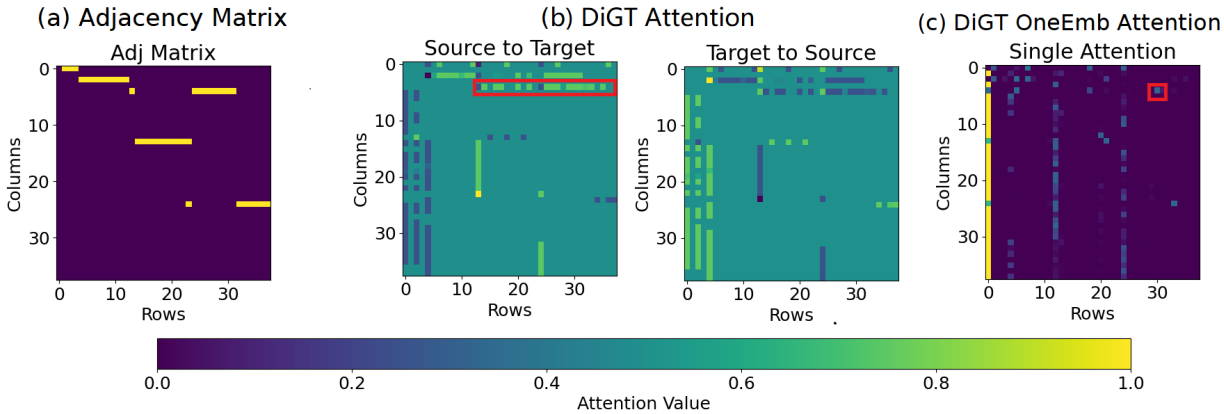

Figure 3: Visualization of the adjacency matrix and the attention matrix for DiGT, for a selected `Malnet-sub` graph.

Traditional transformers struggle to discern critical patterns within a graph. This challenge is shown in Figure 3(c), where the most informative neighboring node for any given source node is indicated by the brightest node in each row. For instance, the red rectangle highlights one such pair. However, this does not necessarily imply that these two nodes are pivotal for the entirety of the figure. On the contrary, in Figure 3(b), the presence of a bright flow within the red rectangle suggests that all these nodes are crucial for the overall graph structure. The application of softmax across the stack direction of the two attention matrices enables the model to discern the relationships between each edge and its corresponding reversed virtual edge within k-hops, and the information flow comes from the union of the original graph and its reversed counterpart.

4.3.2 k-Hop Virtual Edge Filters

Graph transformers, operating under the assumption that all nodes are interconnected, can be interpreted as adding virtual edges among all nodes. We introduce a hyperparameter k to constrain the addition of virtual edges, which has two critical functions: First, it sets the boundary for the shortest directed path distance between two nodes in Equation 2, which contributes to the edge features $\mathbf{B}_{ST}, \mathbf{B}_{TS}$ and gates $\mathbf{G}_{ST}, \mathbf{G}_{TS}$. Second, it determines the $\mathbf{D}_{ST}^{(k)}, \mathbf{D}_{TS}^{(k)}$ virtual edge filters in Equation 6, which restrict message passing among distant nodes. Above, we demonstrated that DiGT effectively captures graph patterns and identifies key node pairs. We now present an ablation study to explore the impact of varying k on the model's performance, where 'unlimited' refers to setting $k = 25$ as a sufficiently large number for the edge embedding layer L_e and not multiplying with $\mathbf{D}_{ST}^{(k)}, \mathbf{D}_{TS}^{(k)}$ filters in Equation 6.

Table 4: *Number of Hops.*

Model	`FlowGraph2`	`FlowGraph3`	`FlowGraph6`	`Twitter3`	`Twitter5`	`Malnet-sub`	`MNIST`	`CIFAR10`
DiGT	98.00 +/- 0.54	**74.61 +/- 1.95**	**46.03 +/- 0.41**	93.33 +/- 0.64	**86.67 +/- 0.52**	**80.78 +/- 1.76**	**98.02 +/- 0.10**	**67.05 +/- 0.20**
DiGT-hop 1	**98.58 +/- 0.24**	74.39 +/- 1.10	43.92 +/- 1.03	**93.90 +/- 0.08**	85.97 +/- 1.35	80.53 +/- 0.87	97.23 +/- 0.28	64.50 +/- 0.84
DiGT-hop 3	98.00 +/- 0.54	**74.61 +/- 1.95**	**46.03 +/- 0.41**	93.33 +/- 0.64	**86.67 +/- 0.52**	80.09 +/- 0.95	**98.02 +/- 0.10**	**67.05 +/- 0.20**
DiGT-hop 5	97.00 +/- 0.71	74.11 +/- 0.98	45.53 +/- 1.27	92.08 +/- 0.56	86.56 +/- 0.25	80.58 +/- 1.15	96.62 +/- 0.48	65.16 +/- 0.94
DiGT-hop 12	96.42 +/- 0.42	70.28 +/- 1.59	44.72 +/- 0.48	92.42 +/- 0.66	85.85 +/- 0.42	**80.78 +/- 1.76**	97.12 +/- 0.22	66.40 +/- 0.12
DiGT-hop unlimited	96.00 +/- 0.71	71.61 +/- 1.17	44.75 +/- 1.37	92.59 +/- 0.58	86.60 +/- 1.69	78.31 +/- 0.74	96.62 +/- 0.45	65.00 +/- 0.10

Figure 4 illustrates that an increase in k leads to more connections among nodes. In Figure 4(b), with $k = 1$, the model behaves similarly to a GNN. It has the ability to capture relationships beyond the adjacency matrix by using additional layers, but it is less effective than with higher k values. Figure 4(d) illustrates a scenario with no hop limitations, allowing unrestricted message passing among all nodes. We can see that the model is capable of reconstructing the graph structure even under the assumption that all nodes are connected. However, the comparison in Table 4 illustrates that DiGT-hop unlimited does not achieve state-

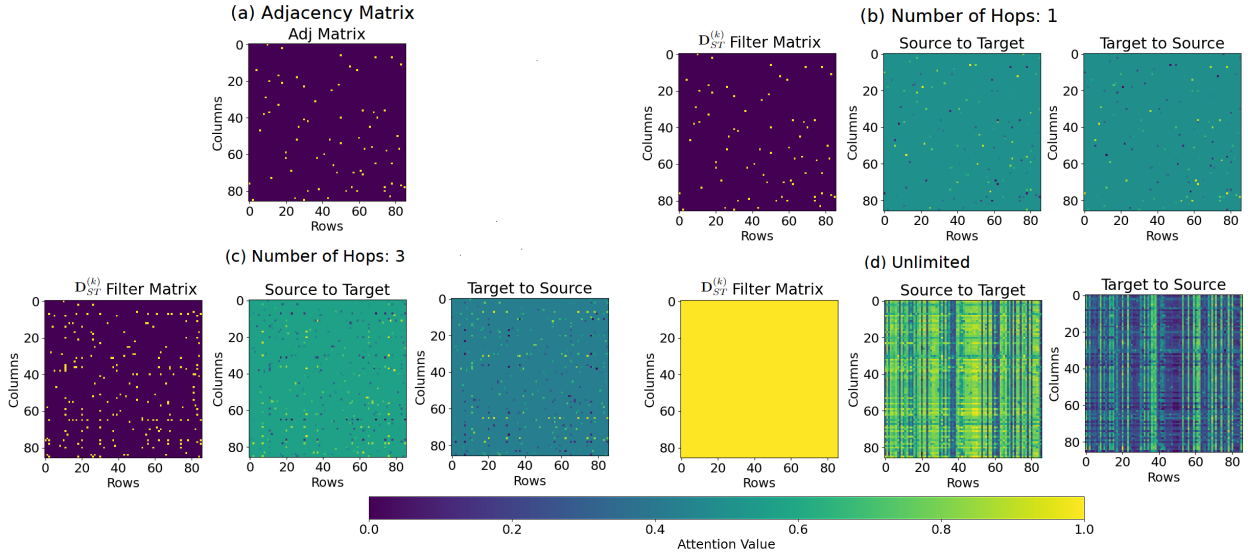

Figure 4: A collection of figures of the DiGT-attention matrix for a selected `FlowGraph6` graph.

of-the-art performance on any datasets. On the other hand, the integration of filter $\mathbf{D}^{(k)}$ matrices, which inform the model about the graph's structure, can effectively improve the model's performance. As seen in Figure 4(c), when $k = 3$, the filter matrices enhance the connectivity of the original graph. Consequently, the attention matrix more accurately reflects important node relationships from the original graph and facilitates effective message passing between distant nodes. This configuration achieves the highest accuracy score on the `FlowGraph6` dataset.

Table 4 further indicates that the optimal number of hops varies with different datasets. For the `Malnet-sub` dataset, the highest accuracy is achieved at $k = 12$, with a significant drop when there are no hop limitations. This can be attributed to the large size of Malnet-sub graphs, which can have up to 2000 nodes, and their edges are sparse. As a result, a model requires a larger k compared to smaller datasets. In contrast, we choose $k = 3$ for other datasets since they only contain approximately 200 nodes per graph. For datasets like `FlowGraph2` and `Twitter3`, $k = 1$ seems more effective, though these results still fall within one standard deviation compared to $k = 3$. In our experiments, we choose $k = 12$ for the `Malnet-sub` dataset and $k = 3$ for other datasets, as the default value.

4.3.3 Hard vs. Soft Thresholding for $\mathbf{D}^{(k)}$

Our k-hop virtual filter matrix $\mathbf{D}^{(k)}$ has been defined as $\mathbf{D}^{(k)}_{i,j} = \{1 \textit{ iff } \delta_{ij} \leq k, 0 \textit{ iff } \delta_{ij} > k\}$ where δ_{ij} denotes the shortest path distance from node i to node j. In this case, 0 means there are no existing paths among two nodes. In this ablation study, we turn our focus to a variant definition, where $\mathbf{D}^{(k)}_{i,j} = \{1 \textit{ iff } \delta_{ij} \leq k, -\infty \textit{ iff } \delta_{ij} > k\}$ to examine how the performance is affected when we set an extreme value for those node pairs with no existing paths.

Table 5: *Ablation:* $\mathbf{D}^{(k)}$

Model	`FlowGraph2`	`FlowGraph3`	`FlowGraph6`	`Twitter3`	`Twitter5`	`Malnet-sub`	`MNIST`	`CIFAR10`
DiGT	**98.00 +/- 0.54**	**74.61 +/- 1.95**	**46.03 +/- 0.41**	**93.33 +/- 0.64**	**86.67 +/- 0.52**	**80.78 +/- 1.76**	**98.02 +/- 0.10**	**67.05 +/- 0.20**
DiGT-inf	92.08 +/- 0.59	69.22 +/- 0.91	37.53 +/- 1.26	91.17 +/- 0.85	84.10 +/- 1.67	75.09 +/- 1.09	93.52 +/- 0.95	49.34 +/- 0.73

Table 5 shows the results for DiGT and its variant, DiGT-inf. We see that on dense graphs like `Twitter`, the accuracy difference between these two methods is small (e.g., at most 1.57% on the `Twitter5`). In contrast, on sparse graphs such as `FlowGraph` and `Malnet-sub`, the DiGT-inf variant results in a significant

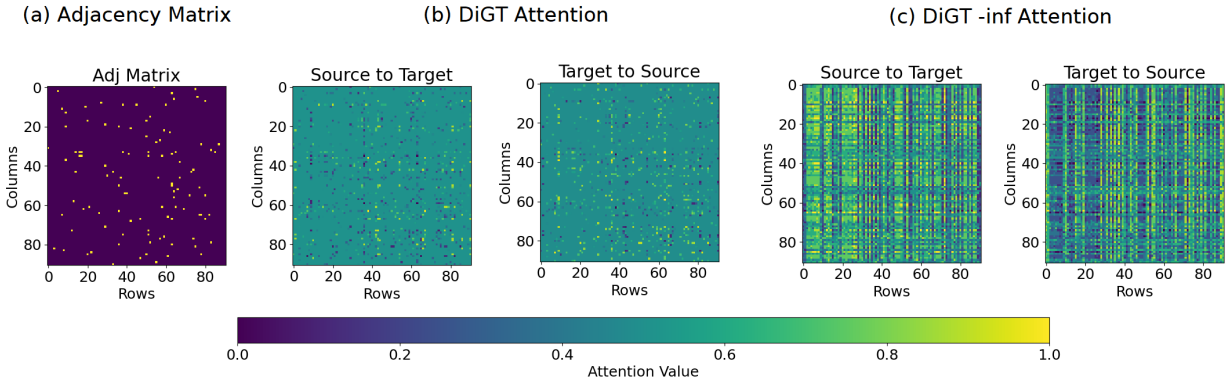

Figure 5: DiGT and DiGT-inf attention matrices for a selected `FlowGraph6` graph.

Table 6: *An Example of Attention Values Before and After Applying softmax*

Relationship	Before softmax		After softmax	
	DiGT	DiGT-inf	DiGT	DiGT-inf
Unconnected	0, 0	$-\infty$, $-\infty$	0.5,0.5	0.5,0.5
Bi-directional	0.7,0.4	0.7,0.4	0.57, 0.43	0.57, 0.43
Uni-directional	0.7,0	0.7,$-\infty$	0.67, 0.33	1.0, 0.0

decline in performance (e.g., a 5.69% drop on `Malnet-sub`). To better understand the results, Table 6 presents an example of attention values, for a pair of nodes, before and after applying the softmax along the stack dimension in our directional attention approach. For an arbitrary node pair, there are three possible relationships: unconnected, bidirectional, or unidirectional. Both models exhibit identical results for pairs that are either unconnected or bi-directional. The divergence occurs with uni-directional connection: DiGT assigns an extreme value of $-\infty$, where as DiGT uses 0. Consequently, DiGT-inf yields a pair $(1.0, 0.0)$ making the attention values solely dependent on one direction (in this case, from source to target). Figure 5 illustrates this effect. In other words, for unidirectional node pairs, a hard thresholding using $-\infty$ blocks information flow completely in one direction (with the non-existent edge), whereas using soft thresholding of 0 still favors the direction that exists, but also allows flow in the opposite direction, which leads to SOTA peformance of DiGT.

5 Conclusions and Future Work

In this paper, we present DiGT, a novel architecture for capturing graph directionality using transformers. We empirically evaluate its classification accuracy on real and synthetic graph datasets and demonstrate its performance gains against state-of-the-art Graph Transformers and Graph Neural Networks. We observe very interesting ablation patterns demonstrating the need for a balanced treatment between local and global attention in node and edge encoding channels.

Our experiments promote the view that GNNs and GTs could be complementary with the shortcomings of the former (over-smoothing, over-squashing, and limited expressiveness) mitigated by the strengths of the latter and vice versa (with scalability limitations, non-standard graph encodings for attention bias, as potential pitfalls in GTs). In the future, to overcome the limitations of moderate-sized graph data that are imposed by the quadratic attention complexity, i.e., to scale up the attention mechanism, we plan to explore recently proposed approaches to expand the context (Bertsch et al., 2023; Tay et al., 2022), and study their effectiveness for (directed) graph datasets.

References

Radhakrishna Achanta, Appu Shaji, Kevin Smith, Aurelien Lucchi, Pascal Fua, and Sabine Süsstrunk. Slic superpixels compared to state-of-the-art superpixel methods. *IEEE transactions on pattern analysis and*

machine intelligence, 34(11):2274–2282, 2012.

Dominique Beaini, Saro Passaro, Vincent Létourneau, Will Hamilton, Gabriele Corso, and Pietro Liò. Directional graph networks. In *International Conference on Machine Learning*, pp. 748–758. PMLR, 2021.

Amanda Bertsch, Uri Alon, Graham Neubig, and Matthew R Gormley. Unlimiformer: Long-range transformers with unlimited length input. *arXiv preprint arXiv:2305.01625*, 2023.

Dexiong Chen, Leslie O'Bray, and Karsten Borgwardt. Structure-aware transformer for graph representation learning. In *International Conference on Machine Learning*, pp. 3469–3489. PMLR, 2022.

Gabriele Corso, Luca Cavalleri, Dominique Beaini, Pietro Liò, and Petar Veličković. Principal neighbourhood aggregation for graph nets. *Advances in Neural Information Processing Systems*, 33:13260–13271, 2020.

Mihai Cucuringu, Huan Li, He Sun, and Luca Zanetti. Hermitian matrices for clustering directed graphs: insights and applications. In *International Conference on Artificial Intelligence and Statistics*, pp. 983–992. PMLR, 2020.

Vijay Prakash Dwivedi and Xavier Bresson. A generalization of transformer networks to graphs. *AAAI Workshop on Deep Learning on Graphs: Methods and Applications*, 2021.

Vijay Prakash Dwivedi, Chaitanya K Joshi, Thomas Laurent, Yoshua Bengio, and Xavier Bresson. Benchmarking graph neural networks. *arXiv preprint arXiv:2003.00982*, 2020.

Scott Freitas, Yuxiao Dong, Joshua Neil, and Duen Horng Chau. A large-scale database for graph representation learning. *arXiv preprint arXiv:2011.07682*, 2020.

Satoshi Furutani, Toshiki Shibahara, Mitsuaki Akiyama, Kunio Hato, and Masaki Aida. Graph signal processing for directed graphs based on the hermitian laplacian. In *Machine Learning and Knowledge Discovery in Databases: European Conference, ECML PKDD 2019, Würzburg, Germany, September 16–20, 2019, Proceedings, Part I*, pp. 447–463. Springer, 2020.

Simon Geisler, Yujia Li, Daniel J Mankowitz, Ali Taylan Cemgil, Stephan Günnemann, and Cosmin Paduraru. Transformers meet directed graphs. In *International Conference on Machine Learning*, pp. 11144–11172. PMLR, 2023.

Yixuan He, Gesine Reinert, and Mihai Cucuringu. Digrac: Digraph clustering based on flow imbalance. *arXiv preprint arXiv:2106.05194*, 2021.

Weihua Hu, Matthias Fey, Marinka Zitnik, Yuxiao Dong, Hongyu Ren, Bowen Liu, Michele Catasta, and Jure Leskovec. Open graph benchmark: Datasets for machine learning on graphs. *Advances in neural information processing systems*, 33:22118–22133, 2020.

Md Shamim Hussain, Mohammed J Zaki, and Dharmashankar Subramanian. Global self-attention as a replacement for graph convolution. In *28th ACM SIGKDD Conference on Knowledge Discovery and Data Mining*, 2022.

Thomas N Kipf and Max Welling. Semi-supervised classification with graph convolutional networks. *arXiv preprint arXiv:1609.02907*, 2016.

Jon M Kleinberg. Authoritative sources in a hyperlinked environment. *Journal of the ACM (JACM)*, 46(5): 604–632, 1999.

Georgios Kollias, Vasileios Kalantzis, Tsuyoshi Idé, Aurélie Lozano, and Naoki Abe. Directed graph auto-encoders. In *Proceedings of the 36th AAAI Conference on Artificial Intelligence (AAAI 2022)*, February 2022.

Devin Kreuzer, Dominique Beaini, Will Hamilton, Vincent Létourneau, and Prudencio Tossou. Rethinking graph transformers with spectral attention. *Advances in Neural Information Processing Systems*, 34: 21618–21629, 2021.

Alex Krizhevsky, Geoffrey Hinton, et al. Learning multiple layers of features from tiny images. 2009.

Jure Leskovec and Julian Mcauley. Learning to discover social circles in ego networks. *Advances in neural information processing systems*, 25, 2012.

Yuankai Luo. Dagformer: Directed acyclic graph transformer. *arXiv preprint arXiv:2210.13148*, 2022.

Mingdong Ou, Peng Cui, Jian Pei, Ziwei Zhang, and Wenwu Zhu. Asymmetric transitivity preserving graph embedding. In *Proceedings of the 22nd ACM SIGKDD international conference on Knowledge discovery and data mining*, pp. 1105–1114, 2016.

Ladislav Rampášek, Michael Galkin, Vijay Prakash Dwivedi, Anh Tuan Luu, Guy Wolf, and Dominique Beaini. Recipe for a general, powerful, scalable graph transformer. *Advances in Neural Information Processing Systems*, 35:14501–14515, 2022.

Guillaume Salha, Stratis Limnios, Romain Hennequin, Viet-Anh Tran, and Michalis Vazirgiannis. Gravity-inspired graph autoencoders for directed link prediction. In *Proceedings of the 28th ACM International Conference on Information and Knowledge Management*, pp. 589–598, 2019.

Hamed Shirzad, Ameya Velingker, Balaji Venkatachalam, Danica J Sutherland, and Ali Kemal Sinop. Exphormer: Sparse transformers for graphs. In *International Conference on Machine Learning*, 2023.

Jiankai Sun, Bortik Bandyopadhyay, Armin Bashizade, Jiongqian Liang, P Sadayappan, and Srinivasan Parthasarathy. Atp: Directed graph embedding with asymmetric transitivity preservation. In *Proceedings of the AAAI Conference on Artificial Intelligence*, pp. 265–272, 2019.

Yi Tay, Mostafa Dehghani, Dara Bahri, and Donald Metzler. Efficient transformers: A survey. *ACM Computing Surveys*, 55(6):1–28, 2022.

Zekun Tong, Yuxuan Liang, Changsheng Sun, Xinke Li, David Rosenblum, and Andrew Lim. Digraph inception convolutional networks. *Advances in Neural Information Processing Systems*, 33, 2020a.

Zekun Tong, Yuxuan Liang, Changsheng Sun, David S Rosenblum, and Andrew Lim. Directed graph convolutional network. *arXiv preprint arXiv:2004.13970*, 2020b.

Ashish Vaswani, Noam Shazeer, Niki Parmar, Jakob Uszkoreit, Llion Jones, Aidan N Gomez, Łukasz Kaiser, and Illia Polosukhin. Attention is all you need. *Advances in neural information processing systems*, 30, 2017.

Petar Veličković, Guillem Cucurull, Arantxa Casanova, Adriana Romero, Pietro Lio, and Yoshua Bengio. Graph attention networks. *arXiv preprint arXiv:1710.10903*, 2017.

Chengxuan Ying, Tianle Cai, Shengjie Luo, Shuxin Zheng, Guolin Ke, Di He, Yanming Shen, and Tie-Yan Liu. Do transformers really perform badly for graph representation? *Advances in Neural Information Processing Systems*, 34:28877–28888, 2021.

Jiawei Zhang, Haopeng Zhang, Congying Xia, and Li Sun. Graph-bert: Only attention is needed for learning graph representations. *arXiv preprint arXiv:2001.05140*, 2020.

Xitong Zhang, Yixuan He, Nathan Brugnone, Michael Perlmutter, and Matthew Hirn. Magnet: A neural network for directed graphs. *Advances in Neural Information Processing Systems*, 34:27003–27015, 2021.

Chang Zhou, Yuqiong Liu, Xiaofei Liu, Zhongyi Liu, and Jun Gao. Scalable graph embedding for asymmetric proximity. In *Proceedings of the AAAI Conference on Artificial Intelligence*, 2017.